Combined Quantum Mechanics (TDDFT) and Classical Electrodynamics (Mie Theory) Methods for Calculating Surface Enhanced Raman and Hyper-Raman Spectra

ARTICLE *in* THE JOURNAL OF PHYSICAL CHEMISTRY A · SEPTEMBER 2012

Impact Factor: 2.69 · DOI: 10.1021/jp307003p · Source: PubMed

4 AUTHORS, INCLUDING:

Jonathan Michael Mullin
Northwestern University
10 PUBLICATIONS **289** CITATIONS
SEE PROFILE

Martin G Blaber
Seagate Technology
36 PUBLICATIONS **906** CITATIONS
SEE PROFILE

THE JOURNAL OF PHYSICAL CHEMISTRY A

Article

pubs.acs.org/JPCA

Combined Quantum Mechanics (TDDFT) and Classical Electrodynamics (Mie Theory) Methods for Calculating Surface Enhanced Raman and Hyper-Raman Spectra

Jonathan Mullin, Nicholas Valley, Martin G. Blaber, and George C. Schatz*

Department of Chemistry, Northwestern University, 2145 Sheridan Road, Evanston, Illinois 60208-3113, United States

Supporting Information

ABSTRACT: Multiscale models that combine quantum mechanics and classical electrodynamics are presented, which allow for the evaluation of surface-enhanced Raman (SERS) and hyper-Raman scattering spectra (SEHRS) for both chemical (CHEM) and electrodynamic (EM) enhancement mechanisms. In these models, time-dependent density functional theory (TDDFT) for a system consisting of the adsorbed molecule and a metal cluster fragment of the metal particle is coupled to Mie theory for the metal particle, with the surface of the cluster being overlaid with the surface of the metal particle. In model A, the electromagnetic enhancement from plasmon-excitation of the metal particle is combined with the chemical enhancement associated with a static treatment of the molecule−metal structure to determine overall spectra. In model B, the frequency dependence of the Raman spectrum of the isolated molecule is combined with the enhancements determined in model A to refine the enhancement estimate. An equivalent theory at the level of model A is developed for hyper-Raman spectra calculations. Application to pyridine interacting with a 20 nm diameter silver sphere is presented, including comparisons with an earlier model (denoted G), which combines plasmon enhanced fields with gas-phase Raman (or hyper-Raman) spectra. The EM enhancement factor for spherical particles at 357 nm is found to be 10^4 and 10^6 for SERS and SEHRS, respectively. Including both chemical and electromagnetic mechanisms at the level of model A leads to enhancements on the order of 10^4 and 10^9 for SERS and SEHRS.

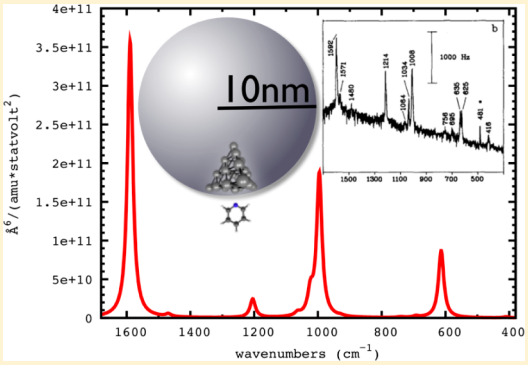

1. INTRODUCTION

Surface enhanced raman scattering (SERS) provides unique capabilities for characterizing molecules at interfaces, and as such, it has seen important applications in surface science and analysis and, increasingly, in medical diagnostics.[1−8] However, the interplay of electromagnetic and electronic structure effects involved in SERS provides important challenges to theory, so it is perhaps not surprising that there have been ongoing theoretical and computational activities, as has been reviewed.[9−17] The SERS enhancement is thought to come from a combination of two mechanisms, chemical (CHEM) enhancement and electromagnetic (EM) enhancement. CHEM enhancement arises from electronic structure changes when a molecule interacts with a metal surface, including charge transfer in both ground and excited states. The EM enhancement is believed to be dominant, so often the chemical enhancement is ignored.[18] The EM enhancement arises from coupling of the external radiation to surface-plasmon excitations at the metal−dielectric interface. These plasmons are collective oscillations of conduction band electrons against the positive ionic background. They can enhance and focus incident light to subwavelength dimensions, below the diffraction limit. Plasmons are associated with enhanced fields near the metal nanoparticle, leading to enhanced Raman scattering from nearby molecules. Further enhancement occurs when scattered photons recouple to the plasmon modes of the metal.

Hyper-Raman scattering (SEHRS) is a nonlinear scattering process in which two photons of incident frequency ω_0 are converted to an outgoing photon of frequency ω that is Raman shifted relative to the second harmonic frequency ($\omega = 2\omega_0 - \Delta\omega$). In bulk solution, the hyper-Raman intensities are often so weak that it is hard to measure spectra. As a result, enhancement factors for SEHRS are not commonly available.[17,19] However, an estimate of the SEHRS enhancement factor of 10^{11} for pyridine was determined by Golab et al.[20] This group also made theory estimates of this enhancement factor using electrodynamics calculations and an earlier generation of electronic structure methods; however, chemical contributions to the enhancement factor were not possible at that time.

SERS enhancement factors are often in the range 10^6−10^8, and if the electromagnetic contribution to the enhancement was dominant, this would be the $|E_{loc}(\omega)|^2\ |E_{loc}(\omega')|^2$, where E_{loc} is the local field enhancement, or approximately $|E_{loc}(\omega)|^4$.[21−23] This approximates the effects of dipole

Received: July 15, 2012
Revised: August 25, 2012
Published: September 4, 2012

reradiation using what is known as the plane-wave approximation, wherein the emitted photon enhancement factor, which involves emission by an induced dipole in the adsorbed molecule at the Stokes frequency, is replaced by the enhancement factor associated with a plane wave interacting with the particle. This approximation as well as the more rigorous theories have been known since the work of Kerker et al.,[24] but only recently these effects have been explicitly explored.[25] The results indicate that the plane-wave approximation is generally adequate in the quasi-static (small particle limit) approximation and even for large particles for observations in certain scattering directions.[25]

The electromagnetic contribution to the SEHRS enhancement factor is nominally $|E_{loc}(\omega)|^4|E_{loc}(\omega')|^2$; however, here the incident and scattered photon frequencies are different enough that typically only one of these is plasmon-enhanced. The EM contribution to the SEHRS enhancement would then be $|E_{loc}(\omega)|^4$ or $|E_{loc}(\omega')|^2$ depending on whether incident or scattered photons are enhanced. Either way, it is clear that the EM contribution to the SEHRS enhancement factor cannot be 10^{11} if the SERS enhancement factor is 10^6-10^8. This suggests that the CHEM enhancement factor for SEHRS is larger than for SERS.[20] The size of the CHEM enhancement factor was explored for SERS in the electronic structure work of Jensen et al.,[26] and for SEHRS by Valley et al.[27] The latter paper showed the importance of the CHEM enhancement for even a qualitative understanding of the SEHRS spectrum. However, in that work, the EM enhancement factor was not included in the calculation.

The challenge to build a model incorporating both electrodynamics (ED) and quantum mechanics (QM) into the optical response stems from the order of magnitude difference in length scales between the nanoparticle and molecule that are coupled in the SERS/SEHRS process. As a result, theoretical treatments of SERS/SEHRS have usually focused either on the dominant EM enhancement using electrodynamics calculations on the nanoparticle substrate,[11] or they have estimated the CHEM enhancement using a small cluster model of the plasmonic nanoparticles.[12,26]

Previous work on combining QM and ED has considered the ED calculations for the particle in the absence of the analyte combined with plasmonic excitation applied as a constant field to the molecule.[11] Corni and Tomasi explicitly coupled electronic structure calculations for the analyte to an ED calculation for the particle in the frequency domain by including effective charges in the molecular Hamiltonian in the quasi-static approximation.[28] Neuhauser developed a local, two-level random phase approximation model for density matrix evolution. This evaluated the molecular population transfer rate, while the finite-difference time-domain (FDTD) method was used to describe the plasmons.[29] Masiello and Schatz applied a many-body Greens function to plasmon-enhanced molecular absorption.[30] A discrete interaction model/quantum mechanics method to explicitly model nanoparticle interaction has been described by Morton and Jensen.[31,32] Here, an atomistic representation of the nanoparticle provides an explicit model for the optical properties of a molecule interacting with the nanoparticle surface. Lombardi and Birke have presented a theory that is based on evaluating the Kramers–Heisenberg–Dirac formula using wave functions that couple the electronic states of the molecule to those of the metal using Fano theory. This includes chemical effects explicitly, and the results have been used to interpret selection rules in SERS.[10,33,34] Chen and Schatz described a hybrid QM/ED method in the time domain using real time (RT)-TDDFT.[35] In this work, a formalism is presented that couples TDDFT in the frequency domain with the particle modeled by Mie Theory. The RT-TDDFT QM/ED method uses the plane-wave approximation for the "back coupling".[30] More recently, a frequency domain linear response version of this theory has been developed by Mullin and Schatz[36] and applied to calculating SERS spectra for pyridine and rhodamine-6G. In that work, the FDTD method was used for ED evaluation of the field at the molecule, and then, frequency domain TDDFT was used to determine frequency-dependent polarizability derivatives for the molecule, with the molecule taken to be in the gas-phase except for imposing restricted orientations that mimic the molecule on the surface. This approach for the coupling of QM with ED is denoted model G in this article.

Here, we develop new multiscale models for the combination of quantum mechanics and classical electrodynamics for describing surface-enhanced Raman and hyper-Raman spectra for both CHEM and EM enhancement mechanisms. In these models, TDDFT (in the frequency domain) is used for the QM calculation, and Mie theory (restricted to spherical particles) is used for the ED calculations. A new feature is that the surface of a metal cluster is overlaid with the surface of the metal particle to combine the two calculations. In model A, the electric field from plasmon-excitation of the metal particle is combined with the chemical enhancement associated with a static treatment of the molecule–metal structure to determine overall spectra. In model B, the frequency dependence of the Raman spectrum of the isolated molecule is combined with enhancements determined using model A to refine the enhancement estimate and include resonance Raman effects in the molecule. An equivalent theory at the level of model A is developed for hyper-Raman spectra calculations.

The QM/ED models are outlined in section 2, while section 3 describes the computational methodology. Numerical results for pyridine are discussed in section 4 along with the implications of our QM/ED methods to linear and nonlinear optical response and its relation to other methods.

2. MODELS

The models we develop in this article are a few of many that one could imagine developing, wherein one couples electrodynamics calculations to electronic structure calculations. Much of what we are considering is guided by SERS and SEHRS experiments, wherein the molecules being studied are either directly on the metallic surface or spaced away from it by a few nanometers at most. In addition, the molecular concentrations are assumed low enough that the plasmonic response of the metal particle is not significantly perturbed by adsorbed molecules, and therefore, the "back coupling" of the excited molecules on the metal particle response can be greatly simplified. However, we do want to include the possibility that the molecule might have resonant excitations. It is generally observed that the overall enhancement for SERS in these circumstances is just the product of the EM and resonance enhancement factors. We will consider theories where that result is assumed. Another issue concerns the use of cluster models, wherein the metal particle is replaced by a metal cluster with a small number of atoms, such as the 20 atom cluster that we mostly consider below. Such models have the advantage of incorporating the chemical enhancement effect automatically, which is highly desirable; however, there are some important

challenges and limitations with these models that dictate how we are forced to use them. One issue arises from the presence of charge-transfer excited states associated with molecule to metal or metal to molecule transitions. Such transitions do occur, but TDDFT substantially underestimates their energies due to self-interaction errors, and this leads to unphysical artifacts, such as low energy excited states.[37] Another problem is that the plasmon excitation in the metal clusters occurs at an energy that is only approximately the same as the much larger metal particle that one is trying to model. Although it has been demonstrated that electronic structure and continuum theories do become the same in the infinite particle limit and taking the particle shapes to be the same,[38] in practical applications these estimates of the plasmon energies can be separated by 1 eV.

To deal with these issues in a practical way, we introduce an overlay approach in which the metal surface of the molecule−metal cluster structure used for electronic structure calculations is matched to the position of the metal nanoparticle used for the electrodynamics calculations. The molecule−cluster electronic structure calculation is used to determine only the static part of the SERS enhancement factor, in this case, using the approach of Morton et al.[9,26] Then, in what we call model A, electrodynamics calculations for the nanoparticle (with no molecule) are used to calculate the EM enhancement at the position of the molecule, taking the molecule−surface distance to be the same as in the molecule−cluster structure. Figure 1

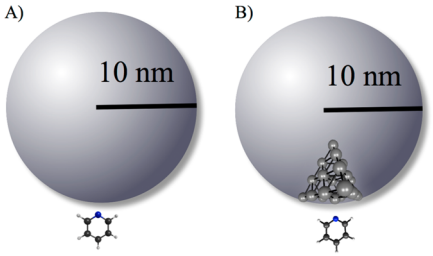

Figure 1. Diagram of the combined quantum mechanics/electrodynamics (QM/ED) model systems. (A) Gas phase molecule treated by quantum mechanics and a particle described by electrodynamics. (B) The quantum region is now considered as a molecule and a 20 atom tetrahedron silver cluster. The cluster is embedded in the same physical location as the particle treated by electrodynamics.

compares the structure used previously in model G with that associated with the overlay in model A, here considering pyridine near a spherical particle. Note that the surface of the metal particle is assumed to be coincident with the nuclei in the cluster atoms that are closest to the molecule. Using model A, the overall enhancement factor is the product of an EM enhancement factor in which the full metal particle and plasmon energy are described, and a CHEM enhancement in which only the static limit of the molecule−cluster system contributes to the spectrum. This treatment avoids double counting of the resonance effects, as the plasmon resonance is included only in the electrodynamics calculations and not the QM calculations.

Model B consists of Model A multiplied by the ratio of the Raman intensity factor for the *isolated* molecule at the frequency being studied to the static Raman intensity. This model therefore incorporates the frequency dependence that the molecular polarizability might have, and even the possibility of resonance Raman enhancement. Any cluster resonance is not included in the molecular resonance calculation due to the problem with self-interaction errors.

Note that, in both models A and B, the molecule orientation relative to the surface is fixed by the ground state structure of the molecule−cluster system. To generate spectra that can be compared with an experiment in which the surface of the nanoparticle is assumed to be fixed in space, but the azimuthal direction of the molecule relative to the polarization of the electromagnetic field is random, we will perform an average of the intensity over azimuthal directions. This is related to what Mullin and Schatz did for model G[36] in which the molecule was taken to be a gas-phase molecule, but with the orientation of the molecule assumed to be fixed relative to the nanoparticle, and also including azimuthal orientation averaging. The present treatment is described in the Supporting Information for both SERS and SEHRS. Note that all the formulas for SEHRS are new.

A feature of model G not present in models A and B is that the distance of the molecule from the nanoparticle surface needs to be fixed as a parameter, rather than being determined by the molecule−cluster calculation. Figure 2A shows the local field magnitude evaluated using Mie theory at 0−5 nm separations between the molecule and a 20 nm diameter silver particle (whose dielectric properties are described later) as a

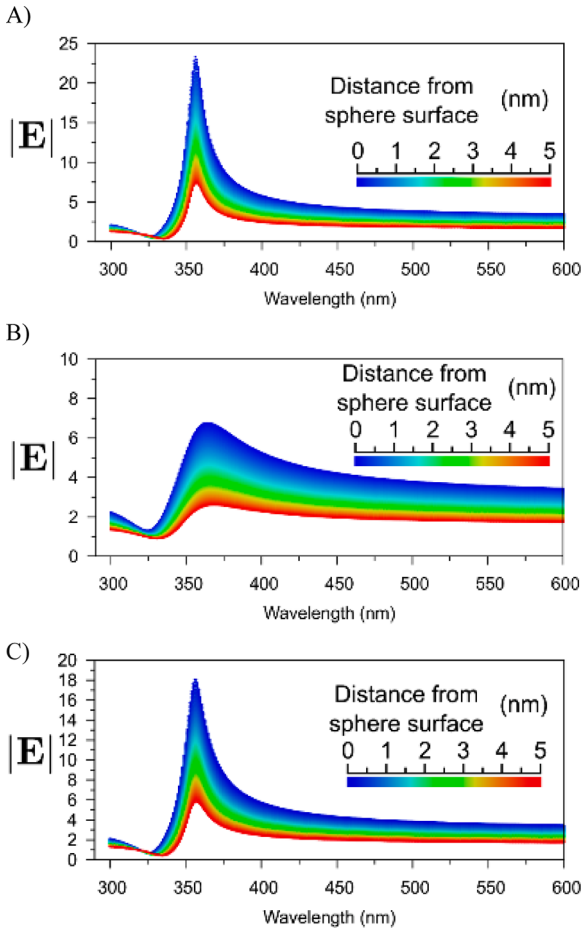

Figure 2. Total field intensity for a 20 nm diameter silver sphere, evaluated at the extinction maximum, 356 nm. The polarization of the field is in the x direction, and the wave propagates in $+z$ direction. (A) Purely elastic electron scattering from the particle surface, (B) purely inelastic, and (C) 10% inelastic.

dx.doi.org/10.1021/jp307003p | J. Phys. Chem. A 2012, 116, 9574−9581

function of wavelength. Especially near the plasmon maximum at 357 nm, the intensity increases rapidly as distance decreases, with a maximum value of |E| = 23 on the surface at the plasmon maximum, but dropping to |E| = 8 at 5 nm separation. This shows that the enhancement factor based on this model is very sensitive to the choice of separation. This means that removing this ambiguity as we do in models A and B is important.

Another point of importance in these models concerns the electrodynamics method used to calculate the electric field at the position of the molecule. The results in Figure 2 are based on Mie theory, which provides an exact solution of Maxwell's equations, and therefore can be used down to zero separation. This provides an improvement over the FDTD method that was used in earlier work,[36] as fields from FDTD become inaccurate close to the particle surface due to the finite difference approximation. However, a limitation of Mie theory is that it can only be used for spherical particles, or for assemblies of spheres, so for more general particles, one is forced to use a numerical method.

As a summary, the three models considered are

(1) QM/ED (G): gas phase QM region, treated as frequency dependent, interacts with the ED region. Orientation/polarization averaging mimics the surface environment.
(2) QM/ED (A): QM used to determine static response of molecule−metal cluster is combined with ED for the overlaid molecule−particle model. Orientation/polarization averaging is similar to model G.
(3) QM/ED (B): QM used to determine frequency dependent molecular Raman spectrum is combined with enhancement factor from model A.

A detailed description of the formulas used for these models is provided in the Supporting Information.

3. COMPUTATIONAL METHODS

3.1. Electrodynamics: Mie Theory of Spheres. The calculation of the field for spheres is performed with a locally developed Mie theory code. The silver dielectric parameters used are those from Johnson and Christy.[39] The results in Figure 2A refer to calculations where the silver dielectric constant is assumed to be size independent. However, for particles this small or smaller, electron scattering from the nanoparticle surface becomes a possibly important source of electron dephasing. Figure 2B,C shows field results in which the imaginary part of the dielectric constant has been modified to include a factor Av_F/R in the Drude expression for the plasmon width, where v_F is the Fermi velocity, R is the particle radius, and A is an empirical parameter set equal to 1.0 in Figure 2B and 0.1 in Figure 2C. The result in Figure 2C has sometimes been taken to be the most realistic, so that is what we will use for the rest of this article. A more complete description of the considerations associated with surface scattering is included in the Supporting Information.

3.2. Quantum Mechanics: Time-Dependent Density Functional Theory (TDDFT). The quantum mechanical calculations presented in this work have been performed using the Amsterdam Density Functional (ADF) program package.[40] Full geometry optimization and frequency calculations for the pyridine−Ag_{20} complex were completed using the Perdew−Wang (PW91) XC-potential and a triple-ζ polarized Slater-type (TZP) basis set. A gradient convergence of 10^{-4} and energy convergence of 10^{-5} were used. Polarizabilities and hyperpolarizabilities were calculated with the AOResponse and Response modules respectively, and using the asymptotically correct statistical average of orbital potential (SAOP) model XC-potential. SAOP has been designed to give accurate excited state properties, allowing for the calculation of accurate response properties.[41] An even-tempered quadruple-ζ plus triple polarization (ET-QZ3P) polar basis set was used for C, H, and N, while a TZP basis set was used for Ag. Scalar relativistic effects were accounted for with the zeroth order regular approximation (ZORA). Polarizabilities on resonance were calculated using a global damping parameter of Γ = 0.004 au (0.1 eV); this is the same as was used in earlier work[37] and is thought to represent a reasonable estimate of the excited state dephasing lifetime. MacMolPlt has been used for visualization of structures and vibrational modes.[42]

4. RESULTS AND DISCUSSION

4.1. Raman Spectra of Pyridine: Gas Phase and QM/ED(G) Results. Pyridine has well studied surface enhanced Raman scattering (SERS) and surface enhanced hyper-Raman scattering (SEHRS) spectra, which have been used for validation of previous theoretical calculations of optical properties. The normal modes that have the largest Raman intensity are 983 cm^{-1} and 1026 cm^{-1} (based on gas-phase DFT calculations with parameters noted above), which both are ring breathing modes. The secondary mode at 598 cm^{-1} is an example of a ring deformation mode. Ring stretching modes appear at 1208 cm^{-1}, 1472 cm^{-1}, and 1583 cm^{-1}. These are about 10 cm^{-1} lower than experimental numbers for SERS;[20] however, other environmental effects such as the presence of the surface or solvent are not considered in our numbers.[9] The calculated 598, 1026, and 1583 cm^{-1} modes are strongly enhanced in the SEHRS spectrum. In past work, both SERS and SEHRS calculated spectra have a weaker 1204 cm^{-1} mode than is seen experimentally.[19,20,27]

The simulated gas phase normal Raman spectrum of pyridine using static polarizability derivatives is shown in Figure 3. A wavelength of 514.5 nm has been assumed in calculating this result, which was a commonly used wavelength in early SERS experiments and calculations. As expected, the main two peaks are at 1026 and 983 cm^{-1}. Relatively less intense peaks are seen

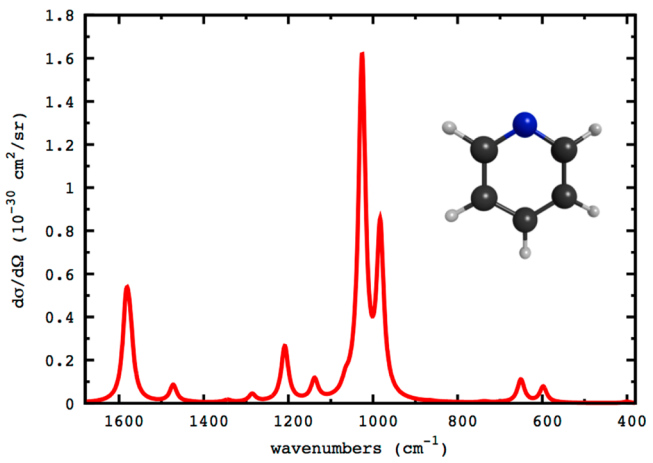

Figure 3. Simulated gas phase normal Raman spectrum of pyridine using static polarizability derivatives. Differential cross-section is given in units of 10^{-30} cm^2/sr and is calculated assuming an incident wavelength of 514.5 nm. Peaks are broadened by a Lorentzian with a full-width at half-maximum of 10 cm^{-1}.

dx.doi.org/10.1021/jp307003p | J. Phys. Chem. A 2012, 116, 9574−9581

at 1583, 1472, 1208, 651, and 598 cm^{-1}. Absolute intensities are similar to that reported in earlier work, but with small differences arising from differences in density functionals, wavelength of evaluation, and other parameters.[27] The appearance of the spectra is similar to that found in experiment.[20] To study the frequency dependence of the polarizability derivatives, in Figure 4, we present the pyridine

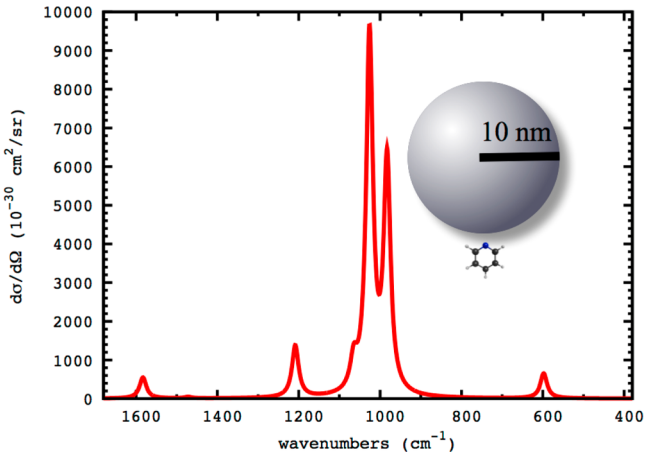

Figure 4. Simulated model G SERS spectrum of pyridine at a separation of 1 nm from a 20 nm diameter silver sphere at an incident wavelength of 357 nm. The differential cross-section is given in units of 10^{-30} cm^2/sr. Peaks are broadened by a Lorentzian with a full-width at half-maximum of 10 cm^{-1}.

gas phase spectrum at 357 nm, which is a wavelength that will be important later in the article as it corresponds to the plasmon resonance frequency of small silver spheres. This wavelength is well to the red of the pyridine electronic states so the spectrum differs only modestly from the static spectrum.[27] However, the magnitude of the intensities is about a factor of 2 higher.

Previous work had looked at using the QM/ED model G method with FDTD for Raman spectra.[35] This article presents model G results where all the polarization enhanced fields are described by Mie theory. Figure 4 shows a QM/ED (G) spectrum for 0.25 nm molecule–sphere separation and for a wavelength of 357 nm. The spectrum is similar to what was presented previously, but the 1589 cm^{-1} mode is less enhanced relative to the ring breathing modes. This indicates that the improved electrodynamics obtained from Mie theory modifies the results compared to what we obtained from FDTD. The integrated enhancement in Figure 5 is 10^4, which is a typical enhancement factor for this wavelength.

4.2. Raman Spectra of Pyridine: QM/ED(A) and QM/ED(B) Results Based on Ag_{20}–Pyridine Surface Complex. We first consider the QM/ED(A) model to include CHEM effects based on a tetrahedral 20 atom silver cluster (Ag_{20}). The possible binding sites of pyridine on Ag_{20} were previously studied by Zhao et al.[37] Here, we consider the static S-complex, where pyridine binds on the (111) surface as this is expected to be a commonly found surface adsorption structure. The geometry of this complex and its relation to the silver particle is shown in the inset to Figure 1B. The system consists of a 20 nm silver sphere with an embedded 20 atom silver tetrahedron where the vertex point opposite to the binding surface is along the *x*-axis. The pyridine is in the *xy* plane bound to the surface of the 20 atom silver tetrahedron with the N atom along the *x*-

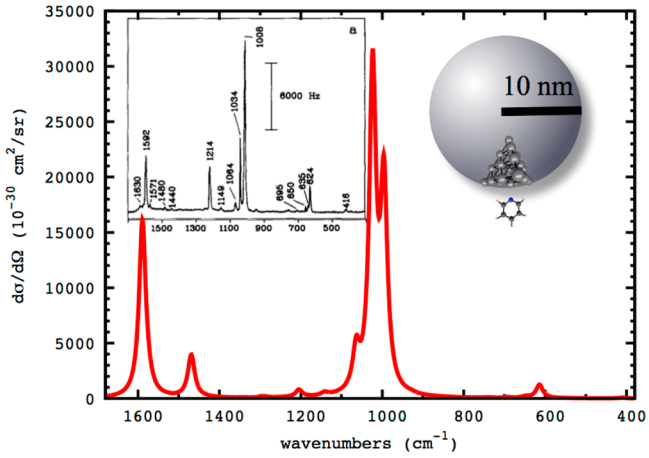

Figure 5. Simulated model A SERS spectrum, using the S-complex overlaid on a 20 nm diameter silver sphere. Differential cross-section is given in units of 10^{-30} cm^2/sr and is calculated assuming an incident wavelength of 357 nm. Peaks are broadened by a Lorentzian with a full-width at half-maximum of 10 cm^{-1}. Inset: experimental spectrum reproduced with permission from ref 20.

axis nearest the (111) surface of the tetrahedron. Since there are only tiny changes in the vibrational mode frequencies for pyridine–Ag_{20} compared to the gas-phase frequencies, we continue to use the gas-phase frequencies to label the modes.

Figure 5 presents the model A results. We see that the relative intensities of the 1589, 1023, and 996 cm^{-1} modes are enhanced in the S-complex compared to that in Figure 3, leading to a spectrum that is in better agreement with the SERS measurement (which is shown in the inset). Also note that the absolute intensity in Figure 5 is about a factor of 3 larger than is obtained from the equivalent model G calculation (not shown), indicating that the CHEM enhancement factor is on the order of 3. Of course the EM enhancement factor is still $\sim 10^4$ as with model G.

Figure 6 illustrates the model B spectrum. Here, the frequency dependent polarizability derivatives for pyridine are evaluated at 357 nm (same as in Figure 4) thereby matching the plasmon frequency of the 20 nm silver particle used for the

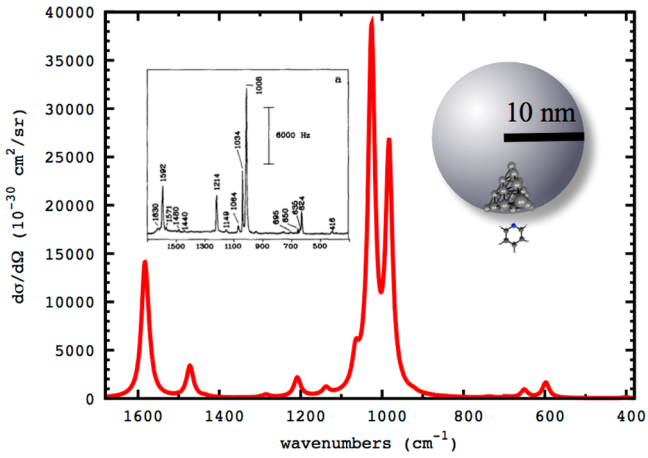

Figure 6. Simulated model B SERS spectrum at an incident wavelength of 357 nm. The differential cross-section is given in units of 10^{-30} cm^2/sr. Peaks are broadened by a Lorentzian with a full-width at half-maximum of 10 cm^{-1}. Inset: experimental spectrum reproduced with permission from ref 20.

dx.doi.org/10.1021/jp307003p | J. Phys. Chem. A 2012, 116, 9574–9581

Mie theory calculation. Compared to the static case in Figure 5, the 613 cm^{-1} mode has a higher relative intensity, while the 989 cm^{-1} has lower relative intensity. The relative intensities of the peaks are very similar to the experiments, except for the 1205 cm^{-1} peak, which is weaker than was seen experimentally. The enhancement factor for the complete system is still on the order of 10^4.

4.3. Hyper-Raman Spectra of Pyridine: Gas Phase and QM/ED(G) Results. The gas phase NHRS spectrum of pyridine is shown in Figure 7. This simulated normal hyper-

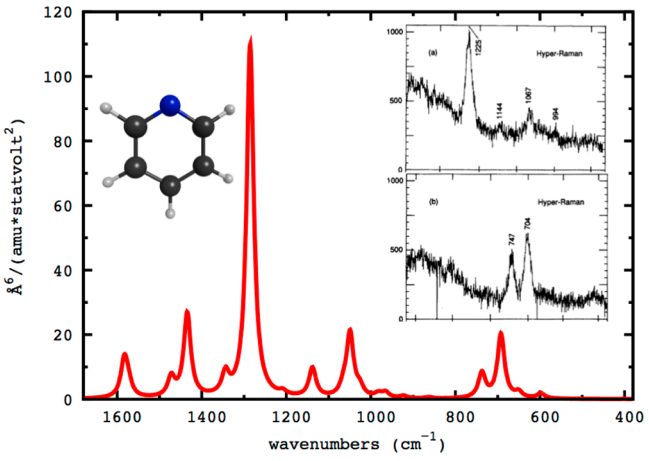

Figure 7. Simulated gas phase normal hyper-Raman spectrum of pyridine using static hyperpolarizability derivatives. Intensities are given in $Å^6/(amu\ statvolt^2)$. Peaks are broadened by a Lorentzian with a full-width at half-maximum of 10 cm^{-1}. Inset: Inset: experimental spectrum reproduced with permission from ref 43.

Raman spectrum has been calculated using static hyperpolarizability derivatives of pyridine. The experimental results[43] are for an incident wavelength of 532 nm. Peaks at 1290, 1141, 1058, 740, and 693 cm^{-1} are seen in both the calculated and experimental results. Both show the asymmetric ring stretch at 1290 cm^{-1} to be the most intense peak. The out-of-plane vibrations at 740 and 693 cm^{-1} are not as intense in the calculation. Further, the higher wavenumber modes at 1472 and 1589 cm^{-1} are not seen experimentally, though this could be a signal issue with the weak hyper-Raman intensity.

To do a QM/ED(G) calculation, the pyridine is placed at 0.25 nm separation from the 20 nm silver sphere. The resulting calculation (not shown) bears little resemblance to the inset of the normal hyper-Raman experimental results in Figure 7 or to the SEHRS experimental results in the inset of Figure 8. This points to the chemical effect as having a large contribution to the SEHRS spectrum, as previously suggested,[27] but here quantified. Clearly, to calculate a combined QM/ED-SEHRS spectrum, chemical effects must be considered.

4.4. Hyper-Raman Spectra of Pyridine: QM/ED(A) Results Based on Ag_{20}−Pyridine Surface Complex. Now we consider QM/ED(A) hyper-Raman spectra based on the Ag_{20}−pyridine complex. Only the static case (model A) is done due to a limitation in the capabilities of the ADF code used for these calculations (which can only calculate static hyperpolarizabilities). As was the case for the SERS calculation, the QM/ED(A) calculation will allow both the CHEM and EM enhancement to be described without double counting the EM enhancement.

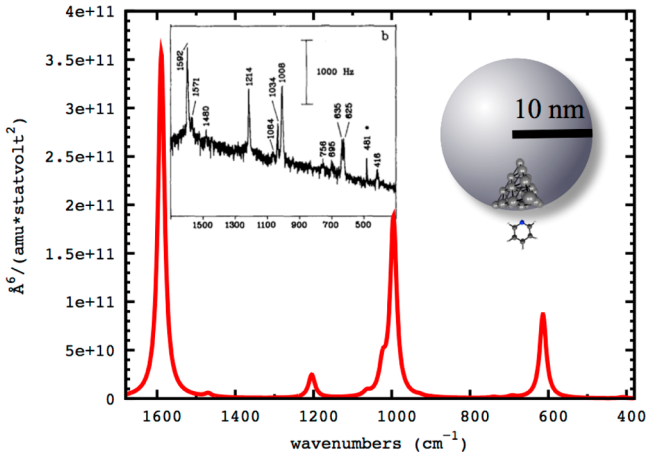

Figure 8. Simulated model A SEHRS spectrum of pyridine using the S-complex. Intensities are given in $Å^6/(amu\ statvolt^2)$. Peaks are broadened by a Lorentzian with a full-width at half-maximum of 10 cm^{-1}. Inset: experimental spectrum reproduced with permission from ref 20.

Figure 8 shows the QM/ED (A) SEHRS spectrum using the same structure as considered in the SERS calculations. This shows that the most intense mode is the symmetric ring stretch at 1589 cm^{-1}. The ring breathing mode at mode 996 cm^{-1} is the next strongest, while the other ring breathing mode at 1023 cm^{-1} is weaker, appearing as a shoulder. The 614 cm^{-1} ring deformation mode is also strongly enhanced. Two weaker peaks at 1205 and 1473 cm^{-1} are also seen. The experimental surface enhanced hyper-Raman spectrum of pyridine is in the inset. Comparison with Figure 7 shows that there are major changes in the SEHRS spectrum compared to the NHRS spectrum and that model A correctly describes these changes. Model A does not hit every mode correctly, for example, the 1205 cm^{-1} mode is stronger in the measured spectrum than is seen in the model A results.

While our model A calculation includes both chemical and electromagnetic contributions to the enhancement, as does the experiment, the frequency dependence of the hyperpolarizability derivatives is not included. Resonant charge transfer effects have been considered for SERS,[33,44] but they are not included in our SEHRS chemical mechanism estimate. This is a further refinement that could be investigated in the future with revisions to the ADF code.

Table 1 summarizes the enhancement factors seen in all the calculations presented. For SERS, the enhancement factor is about 10^4 for all the models we considered, as it is dominated by the EM enhancement. For SEHRS, the chemical enhancement is estimated to be 10^2 from static calculations for the S-complex. Overall the SEHRS enhancement is on the order of 10^9. These results are consistent with the measured enhancement factors of 10^6 and 10^{11} for SERS and SEHRS when one considers that the EM enhancement factor is $\sim 10^2$ smaller at 357 nm than at longer wavelengths (such as 500−800 nm) where the experiments have actually been done. We also note that the SEHRS measurements refer to somewhat ill-defined electrochemically roughened surfaces, so the 20 nm silver spheres are far from ideal for modeling surface enhancement for the measurements we considered.

dx.doi.org/10.1021/jp307003p | J. Phys. Chem. A 2012, 116, 9574−9581

Table 1. Enhancement Factors Based on Models Presented in This Article

Raman	enhancement factor
pyridine (static)	1
pyridine (357 nm)	~2
pyridine QM/ED (static) model G	~10^4
pyridine QM/ED (357 nm) model G	~10^4
S-complex (static)	~2
S-complex (357 nm)	~10^5
S-complex QM/ED (static) model A	~10^4
S-complex QM/ED (357 nm) model B	~10^4
hyper-Raman	**enhancement factor**
pyridine (static)	1
pyridine QM/ED (static) model G	~10^6
S-complex (static)	~10^2
S-complex QM/ED (static) model A	~10^9

5. CONCLUSIONS

The QM/ED models presented here provide a hierarchy of capabilities of general use in modeling SERS and SEHRS intensities. Model G, which was presented earlier, describes only the EM enhancement factor, and there are uncertainties in the positioning of the molecule relative to the nanoparticle surface. It does include orientation and polarization effects that mimic what occurs in the experiments, so in this respect, it is an improvement over simpler arguments that multiply the gas-phase Raman intensities by the local field enhancement factor. Model A goes beyond model G by incorporating the static CHEM enhancement, and it also provides a more seamless determination of the location of the molecule relative to the surface by using an embedding procedure. Model B goes beyond model A by including frequency dependent effects in the molecular polarizability derivatives, and it has the capability of describing surface enhanced resonance Raman processes. Although we only presented a theory of hyper-Raman scattering at the model A and G levels, it is clear that model B could also be implemented if frequency-dependent hyperpolarizability derivatives were included in the ADF electronic structure code.

For each model, there are choices to be made concerning the electrodynamics and quantum mechanics methods and concerning the cluster model used to describe the metal particle. Here, we used Mie theory for the electrodynamics, which has the advantage of being exact but is restricted to spherical particles or clusters thereof. For the QM calculation, we used TDDFT with the PW91 functional. This choice leads to polarizabilities and hyperpolarizabilities with acceptable accuracy, but there are serious problems with self-interaction errors that lead to inaccurate charge transfer excited states. We therefore choose to use frequency-dependent molecular properties only in model B where the metal cluster is left out. The Ag_{20} cluster used in the QM calculations is one of the smallest clusters that can realistically be used, as it provides a (111) surface for the S-complex in which there is just 10 atoms on the surface. Usually chemical interactions are quite short-ranged so larger clusters may not be necessary; however, this is a topic for future study. In addition, future work will also study the effect of averaging the spectra over a distribution of surface sites.

The applications to pyridine that we presented have provided a better picture for the relationship between the gas phase Raman and SERS spectra (and likewise for SEHRS) than was available previously. Thus, in model A, there are changes in the relative SERS intensities of many of the modes compared to model G due to chemical effects, while in model B, one sees further changes that arise from frequency-dependent effects. The changes in SEHRS spectra between models G and A are much more dramatic, as summarized in Table1, showing that it is essential to include chemical effects when describing SEHRS. Note that all of our enhancement estimates are in the zero Stokes shift limit. Including a finite Stokes shift will typically reduce the enhancement by a factor of about 3.

■ ASSOCIATED CONTENT

Supporting Information

(1) Linear response TDDFT, (2) Mie theory, (3) orientation and azimuthal averaging in SERS spectra, (4) orientation and azimuthal averaging in SEHRS spectra, (5) incorporation of surface scattering effect in the metal dielectric function (with parameters provided in Table S1). Plots include (S1) vibrational normal modes of pyridine, (S2) calculated resonance Raman spectra of pyridine, (S3) static Raman spectra of S-complex, (S4) calculated resonance Raman spectra of S-complex, (S5) calculated normal hyper-Raman spectrum of pyridine. This material is available free of charge via the Internet at http://pubs.acs.org.

■ AUTHOR INFORMATION

Corresponding Author

*E-mail: schatz@chem.northwestern.edu.

Notes

The authors declare no competing financial interest.

■ ACKNOWLEDGMENTS

J.M. was supported by DOE SISGR grant DE-SC0001785. N.V. and G.C.S were supported by DOE BES Grant DE-SC0004752. M.G.B. thanks DARPA-DLT N66001-11-1-4179 and NSF MRSEC (Grant No. DMR-1121262). We would like to thank Professor Hanning Chen for useful discussions. This research was supported in part through the computational resources and staff contributions provided by Information Technology at Northwestern University as part of its shared cluster program, Quest.

■ REFERENCES

(1) Jain, P. K.; Huang, X. H.; El-Sayed, I. H.; El-Sayed, M. A. *Acc. Chem. Res.* **2008**, *41*, 1578−1586.
(2) Camden, J. P.; Dieringer, J. A.; Zhao, J.; Van Duyne, R. P. *Acc. Chem. Res.* **2008**, *41*, 1653−1661.
(3) Bell, S. E. J.; Sirimuthu, N. M. S. *Chem. Soc. Rev.* **2008**, *37*, 1012−1024.
(4) Porter, M. D.; Lipert, R. J.; Siperko, L. M.; Wang, G.; Narayanana, R. *Chem. Soc. Rev.* **2008**, *37*, 1001−1011.
(5) Wu, D. Y.; Li, J. F.; Ren, B.; Tian, Z. Q. *Chem. Soc. Rev.* **2008**, *37*, 1025−1041.
(6) Kneipp, J.; Kneipp, H.; Kneipp, K. *Chem. Soc. Rev.* **2008**, *37*, 1052−1060.
(7) McNay, G.; Eustace, D.; Smith, W. E.; Faulds, K.; Graham, D. *Appl. Spectrosc.* **2011**, *65*, 825−837.
(8) Henry, A. I.; Bingham, J. M.; Ringe, E.; Marks, L. D.; Schatz, G. C.; Van Duyne, R. P. *J. Phys. Chem. C* **2011**, *115*, 9291−9305.
(9) Morton, S. M.; Silverstein, D. W.; Jensen, L. *Chem. Rev.* **2011**, *111*, 3962−3994.
(10) Lombardi, J. R.; Birke, R. L. *Acc. Chem. Res.* **2009**, *42*, 734−742.
(11) Zhao, J.; Pinchuk, A. O.; Mcmahon, J. M.; Li, S.; Ausman, L. K.; Atkinson, A. L.; Schatz, G. C. *Acc. Chem. Res.* **2008**, *41*, 1710−1720.

(12) Jensen, L.; Aikens, C. M.; Schatz, G. C. *Chem. Soc. Rev.* **2008**, *37*, 1061−1073.
(13) Tong, L. M.; Zhu, T.; Liu, Z. F. *Chem. Soc. Rev.* **2011**, *40*, 1296−1304.
(14) Halas, N. J.; Lal, S.; Chang, W. S.; Link, S.; Nordlander, P. *Chem. Rev.* **2011**, *111*, 3913−3961.
(15) Schatz, G. C. *Acc. Chem. Res.* **1984**, *17*, 370−376.
(16) Moskovits, M. *Rev. Mod. Phys.* **1985**, *57*, 783−826.
(17) Metiu, H.; Das, P. *Annu. Rev. Phys. Chem.* **1984**, *35*, 507−536.
(18) Moskovits, M. *J. Raman Spectrosc.* **2005**, *36*, 485−496.
(19) Yang, W.-H.; Schatz, G. C. *J. Chem. Phys.* **1992**, *97*, 3831−3845.
(20) Golab, J. T.; Sprague, J. R.; Carron, K. T.; Schatz, G. C.; Van Duyne, R. P. *J. Chem. Phys.* **1988**, *88*, 7942.
(21) Camden, J. P.; Dieringer, J. A.; Wang, Y.; Masiello, D. J.; Marks, L. D.; Schatz, G. C.; Van Duyne, R. P. *J. Am. Chem. Soc.* **2008**, *130*, 12616−12617.
(22) Khan, S. A.; Senapati, D.; Senapati, T.; Bonifassi, P.; Fan, Z.; Singh, A. K.; Neeley, A.; Hill, G.; Ray, P. C. *Chem. Phys. Lett.* **2011**, *512*, 92−95.
(23) Mullin, J. M.; Autschbach, J.; Schatz, G. C. *Comput. Theor. Chem.* **2012**, *987*, 32−41.
(24) Kerker, M.; Wang, D.; Chew, H. *Appl. Opt.* **1980**, *19*, 4159−4174.
(25) Ausman, L. K.; Schatz, G. C. *J. Chem. Phys.* **2009**, *131*, 084708.
(26) Morton, S. M.; Jensen, L. *J. Am. Chem. Soc.* **2009**, *131*, 4090−4098.
(27) Valley, N.; Jensen, L.; Autschbach, J.; Schatz, G. C. *J. Chem. Phys.* **2010**, *133*, 054103.
(28) Corni, S.; Tomasi, J. *J. Chem. Phys.* **2002**, *116*, 1156−1164.
(29) Lopata, K.; Neuhauser, D. *J. Chem. Phys.* **2009**, *130*, 104707.
(30) Masiello, D. J.; Schatz, G. C. *Phys. Rev. A* **2008**, *78*, 042505.
(31) Morton, S. M.; Jensen, L. *J. Chem. Phys.* **2010**, *133*, 074103.
(32) Morton, S. M.; Jensen, L. *J. Chem. Phys.* **2011**, *135*, 134103.
(33) Lombardi, J. R.; Birke, R. L. *J. Phys. Chem. C* **2008**, *112*, 5605−5617.
(34) Lombardi, J. R.; Birke, R. L. *J. Chem. Phys.* **2012**, *136*, 144704−144711.
(35) Chen, H.; McMahon, J.; Ratner, M.; Schatz, G. *J. Phys. Chem. C* **2010**, *114*, 14384−14392.
(36) Mullin, J.; Schatz, G. C. *J. Phys. Chem. A* **2012**, *116*, 1931−1938.
(37) Zhao, L.; Jensen, L.; Schatz, G. C. *J. Am. Chem. Soc.* **2006**, *128*, 2911−2919.
(38) Aikens, C. M.; Li, S.; Schatz, G. C. *J. Phys. Chem. C* **2008**, *112*, 11272−11279.
(39) Johnson, P. B.; Christy, R. W. *Phys. Rev. B* **1972**, *6*, 4370−4379.
(40) te Velde, G.; Bickelhaupt, F. M.; Baerends, E. J.; Guerra, C. F.; van Gisbergen, S. J. A.; Snijders, J. G.; Ziegler, T. *J. Comput. Chem.* **2001**, *22*, 931−967.
(41) Schipper, P. R. T.; Gritsenko, O. V.; van Gisbergen, S. J. A.; Baerends, E. J. *J. Chem. Phys.* **2000**, *112*, 1344−1352.
(42) Bode, B. M.; Gordon, M. S. *J. Mol. Graphics Modell.* **1998**, *16*, 133−138.
(43) Neddersen, J. P.; Mounter, S. A.; Bostick, J. M.; Johnson, C. K. *J. Chem. Phys.* **1989**, *90*, 4719−4726.
(44) Arenas, J.; Tocon, I.; Otero, J.; Marcos, J. *J. Phys. Chem.* **1996**, *100*, 9254−9261.